Pergamon

0020-7225(93)E0006-Q

Int. J. Engng Sci. Vol. 33, No. 3, pp. 437–446, 1995

0020-7225/95 $9.50 + 0.00

HYDROMAGNETIC TWO-PHASE FLOW IN A CHANNEL

ALI J. CHAMKHA

Department of Mechanical Engineering, Kuwait University, Safat, 13060 Kuwait

Abstract—The problem of hydromagnetic flow of a dusty electrically conducting fluid accounting for particle-phase stresses in a channel is solved in closed form. Graphical steady and time-varying solutions for the volume flow rates and the skin-friction coefficients of both phases for various physical parameters involved in the problem are reported and discussed.

1. INTRODUCTION

The importance of two-phase particulate flows has led to the development of several multiphase theories. These theories are based mainly on either the Eulerian approach or the Lagrangian approach. The former treats both phases as continua with interfacial interactions such as drag and heat transfer (see, for instance Marble [1], Ishii [2] and Soo [3]). The latter approach treats only the fluid as a continuum while the particle phase is governed by the kinetic theory (see, for instance, Berlomont *et al.* [4, 5]). Both approaches have been successfully applied for the analysis and solution of two-phase flow situations. In the present work the Eulerian approach is employed for modeling unsteady hydromagnetic flow of a dusty conducting fluid in a channel.

The model considered herein allows for finite particulate volume fraction, particle-phase viscous stresses and an externally applied transverse magnetic field. Soo [6] and Gadiraju *et al.* [7] have discussed and considered the particle-phase viscous effects which arise from additional shearing due to high particulate concentrations in solid–fluid systems. Physically, as the fluid viscosity represents fluid–fluid interaction, the particle viscosity can be thought of as representing the particle–particle interaction. Mathematically, since the particle cloud is not a continuous system, a continuum description of such a system involves averages over small volume elements and/or small time intervals. The actual variables associated with individual particles will not exactly correspond to those averages. This gives rise to the possibility of transfers of mass, momentum, and energy which are not accounted for by the average variables (see, for instance, Drew [8] and Drew and Segal [9]). The resulting momentum transfer can be modeled as viscous in nature as done herein.

Possibe applications of this type of flow can be found in many industries. For example, in the power industry, among the methods of generating electric power is one in which electric energy is extracted directly from a moving conducting fluid. The simplest way of accomplishing this is to pass the fluid through a pipe or a channel of gradually varying cross-sectional area (see Cramer and Pai [10]). Soot particles can be introduced into the system as a consequence of the corrosion activity that may take place at the walls of the channel (see Soo [11]). When the particle concentration becomes high, additional viscous stresses are brought about due to particle interactions. A problem of this nature is quite complex to handle if all MHD effects (such as the Hall effect and induced magnetic field) and particle distribution are all present. To gain insight into the relative influence of the several physical parameters involved in this problem, it is important to obtain closed-form solutions. This can be accomplished by making many simplifications whereby the governing equations reduce to a form that can be solved analytically. This is the purpose of the present work.

The first MHD channel flow was first investigated in 1930 by Hartmann, who considered plane Poiseuille flow with a transverse magnetic field. Carstoiu [12] later reported unsteady solutions for Hartmann flow. Tseng and Sahai [13] investigated the problem of steady

hydromagnetic flow of a particulate suspension between two parallel plates. Ritter and Peddieson [14] discussed transient two-phase flow in a channel without considering the effects of particulate viscous stresses. It is of interest in this paper to generalize the solutions reported by Ritter and Peddieson [14] to include such effects as particle-phase stresses, finite volume fraction, and transverse magnetic field. Analytical steady and transient solutions for the velocity profiles, volume flow rates, and the skin-friction coefficients for both phases will be reported herein. The fluid is assumed to be incompressible and electrically conducting and the particle phase is assumed to be incompressible, electrically nonconducting and pressureless. No applied electric field is assumed to occur and the Hall effect of magnetohydrodynamics is neglected. The motion of the suspension in the channel is assumed to be driven by a constant pressure gradient applied in the x direction parallel to the channel walls. In addition, the flow is assumed fully developed such that the physical variables are independent of the axial coordinate.

2. GOVERNING EQUATIONS

Consider unsteady flow of a dusty conducting fluid in a channel in the presence of a transverse magnetic field. The origin of the x,y Cartesian coordinates is placed in the middle of the channel width with the suspension moving in the x direction. The applied magnetic field is stationary and normal to the flow direction. Figure 1 shows a schematic for the problem under consideration. The Reynolds magnetic number is assumed small so that the induced magnetic field can be neglected as done by previous authors (see Mitra and Bhattacharyya [15]). The particles are assumed to be of one size with uniform volume fraction.

To formulate the governing equations for this investigation, the balance laws of mass and linear momentum are considered along with information about interfacial and external body forces and stress tensors for both phases.

The balance laws of mass (for the fluid and particulate phases, respectively) can be written as

$$\partial_t \phi - \nabla \cdot ((1-\phi)\mathbf{V}) = 0, \qquad \partial_t \phi + \nabla \cdot (\phi \mathbf{V}_p) = 0 \tag{2.1}$$

where t is time, ϕ is the particulate volume fraction, ∇ is the gradient operator, $\mathbf{V}$ is the fluid-phase velocity vector, and $\mathbf{V}_p$ is the particulate-phase velocity vector. The true densities for both phases are assumed constant.

The balance laws of linear momentum (for the fluid and particulate phases, respectively) can be written as

$$\rho(1-\phi)(\partial_t \mathbf{V} + \mathbf{V} \cdot \nabla \mathbf{V}) = \nabla \cdot \underline{\underline{\tau}} - \mathbf{f} + \mathbf{b}, \qquad \rho_p \phi(\partial_t \mathbf{V}_p + \mathbf{V}_p \cdot \nabla \mathbf{V}_p) = \nabla \cdot \underline{\underline{\tau}}_p + \mathbf{f} + \mathbf{b}_p \tag{2.2}$$

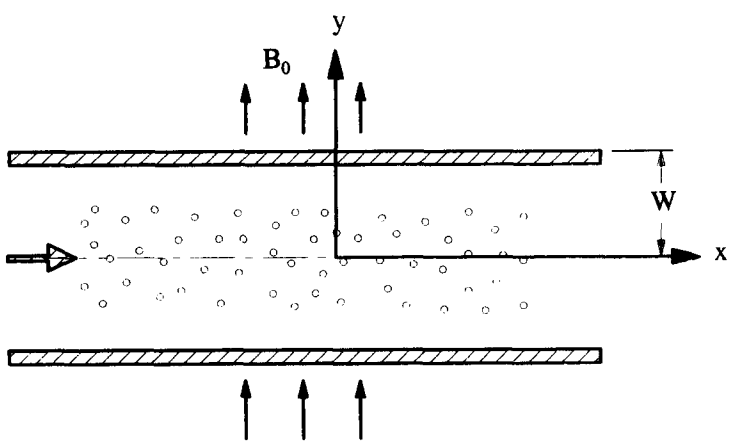

Fig. 1. Problem definition.

where ρ is the fluid-phase density, $\underline{\underline{\sigma}}$ is the fluid-phase stress tensor, $\mathbf{f}$ is the interphase force per unit volume acting on the particle phase, $\mathbf{b}$ is the fluid-phase body force per unit volume, ρ_p is the particle-phase density, $\underline{\underline{\sigma}}_p$ is the particle-phase shear stress, and $\mathbf{b}_p$ is the particle-phase body force per unit volume.

Along with equations (2.1) and (2.2), the following constitutive equations are used

$$\underline{\underline{\sigma}} = (1-\phi)(-P\underline{\underline{I}} + \mu(\phi)(\nabla\mathbf{V} + \nabla\mathbf{V}^T)), \qquad \underline{\underline{\sigma}}_p = \phi\mu_p(\phi)(\nabla\mathbf{V}_p + \nabla\mathbf{V}_p^T)$$
$$\mathbf{f} = N(\phi)\rho_p\phi(\mathbf{V} - \mathbf{V}_p), \qquad \mathbf{b} = -\epsilon/\rho(\mathbf{V}\times\mathbf{B})\times\mathbf{B}, \qquad \mathbf{b}_p = 0 \tag{2.3}$$

where P is the fluid pressure, $\underline{\underline{I}}$ is the unit tensor, μ is the fluid dynamic viscosity, μ_p is the particle-phase dynamic viscosity, N is the inverse relaxation time (the inverse time required by a particle to reduce its velocity relative to that of the fluid by e^{-1} from its initial value (Marble [1]), ϵ in the fluid's electrical conductivity, $\mathbf{B}$ is the magnetic induction field vector, and a superposed T denotes the transpose of a second-order tensor. It should be mentioned that more elaborate multiphase theories which allow for a transition of the particle phase from fluid-like behavior at sufficiently low volume fractions to solid-like behavior at higher volume fractions will eventually be needed for modeling more complex multiphase problems. Endowing the particle phase with viscosity is a step in that direction since at higher volume fractions, the particle-phase behavior approaches that of a rigid body provided μ_p is allowed to increase rapidly with ϕ. In the present work ϕ, ρ, ρ_p, μ, μ_p, and N will all be treated as constants.

Equations (2.1)–(2.3) represent an extension of the dusty-gas model (a model meant for the description of suspensions exhibiting small particulate volume fraction) discussed by Marble [1] to include the particle-phase viscosity and magnetic field effects and is applicable for any size particles. It is convenient to nondimensionalize the governing differential equations given previously by using

$$y = W\eta, \qquad t = (\tau W^2)/\nu, \qquad \mu = \rho\nu, \qquad \mu_p = \rho_p\nu_p, \qquad \rho_p = \kappa\rho(1-\phi)/\phi$$
$$\mathbf{V} = (G_0W^2)/\mu F(\eta,\tau)\mathbf{e}_x, \qquad \mathbf{V}_p = (G_0W^2)/\mu F_p(\eta,\tau)\mathbf{e}_x, \qquad \mathbf{B} = \mathbf{B}_0\mathbf{e}_y \tag{2.4}$$

where B_0 and $G_0 = -\partial_x P$ are constants, W is the channel half width, and $\mathbf{e}_x$ and $\mathbf{e}_y$ are unit vectors in the x and y directions, respectively. Substituting equations (2.3) and (2.4) into equations (2.1) and (2.2) and rearranging yield

$$\partial_\tau F = \partial_{\eta\eta}F + \kappa\alpha(F_p - F) - M^2F + 1 \tag{2.5}$$

$$\partial_\tau F_p = \beta\partial_{\eta\eta}F_p + \alpha(F - F_p) \tag{2.6}$$

where $\alpha = (NW^2)/\nu$, $\beta = \nu_p/\nu$, and $M = (\epsilon/\mu)^{1/2}B_0W$ are the inverse Stoke's number, the viscosity ratio, and the Hartmann number, respectively.

The corresponding dimensionless initial and boundary conditions for this problem are

$$F(\eta,0) = 0, \qquad F_p(\eta,0) = 0, \qquad \partial_\eta F(0,\tau) = 0, \qquad \partial_\eta F_p(0,\tau) = 0$$
$$F(1,\tau) = 0, \qquad F_p(1,\tau) = -\omega\partial_\eta F_p(1,\tau) \tag{2.7}$$

where ω is a slip coefficient. Equations (2.7a) and (2.7b) indicate that the motion of both phases start from rest. Equations (2.7c) and (2.7d) indicate symmetry conditions; that is, the velocity profiles of both phases are symmetrical about the center line of the channel. Equation (2.7e) suggests the fact that the fluid does not slip at the boundaries of the channel. Equation (2.7f), familiar from rarefied gas dynamics, allows for particulate wall slip. The amount of slip is controlled by the coefficient ω. It can be seen from equation (7f) that if ω is equated to zero, a no-slip condition is obtained. However, if ω is made infinite, a perfect slip condition is recovered. In general, ω is a function of the other parameters involved in the problem. No attempt was made herein to do so and ω was assumed to be constant.

The volumetric flow rates and the skin friction coefficients for the fluid and particulate

phases are important physical properties for this type of flow. These are defined in dimensionless form, respectively, as

$$Q = 2\int_0^1 F(\eta, \tau)\,d\eta, \qquad Q_p = 2\int_0^1 F_p(\eta, \tau)\,d\eta, \qquad C = -\partial_\eta F(1, \tau), \qquad C_p = -\beta\kappa\partial_\eta F_p(1, \tau). \tag{2.8}$$

As mentioned before, it is expected that the velocity profiles for both the fluid and particle phases are parabolic in shape and that the maximum fluid and particle velocities occur in the middle of the channel. This is taken into account in equations (2.8).

3. RESULTS AND DISCUSSION

In this section, analytical solutions for the problem under consideration for steady-state and transient conditions will be derived. Numerical computations of the developed solutions will be performed and representative results will be presented graphically to elucidate interesting features of the solutions.

3.1 Steady-state solutions

Under steady-state conditions, the terms on the left-hand side of each of equations (2.5) and (2.6) will vanish. The resulting two equations can be combined into a fourth-order, linear, non-homogeneous, ordinary differential equation. This can be written as

$$\beta F^{iv} - (\beta(M^2 + \kappa\alpha) + \alpha)F'' + \alpha M^2 F = \alpha \tag{3.1}$$

where a prime denotes ordinary differentiation with respect to η. The solution of equation (3.1) subject to the corresponding boundary conditions given in equations (2.7) can be shown to be

$$F(\eta) = A_1 \cosh(m_1\eta) + A_2 \cosh(m_2\eta) + 1/M^2 \tag{3.2}$$

where

$$m_1 = ((\beta(M^2 + \kappa\alpha) + \alpha + ((\beta(M^2 + \kappa\alpha) + \alpha)^2 - 4\beta\alpha M^2)^{1/2})/(2\beta))^{1/2} > 0$$
$$m_2 = ((\beta(M^2 + \kappa\alpha) + \alpha - ((\beta(M^2 + \kappa\alpha) + \alpha)^2 - 4\beta\alpha M^2)^{1/2})/(2\beta))^{1/2} > 0 \tag{3.3}$$

$$A_2 = ((c_1 - 1)\omega\cosh(m_1) + c_1 m_1 \sinh(m_1))/(M^2(c_2\cosh(m_1)(\omega\cosh(m_2) + m_2\sinh(m_2)) - c_1\cosh(m_2)(\omega\cosh(m_1) + m_1\sinh(m_1)))) \tag{3.4}$$

$$A_1 = -(A_2\cosh(m_2) + 1/M^2)/\cosh(m_1), \qquad c_i = 1 + (M^2 - m_i^2)/(\kappa\alpha), \qquad i = 1,2.$$

The corresponding solution for F_p is found to be

$$F_p(\eta) = A_1 c_1 \cosh(m_1\eta) + A_2 c_2 \cosh(m_2\eta) + 1/M^2. \tag{3.5}$$

With the velocity fields for both phases known, the solutions for the volumetric flow rates and the skin-friction coefficients for both the fluid and particle phases can now be determined. This is done by using equations (2.8) and performing the appropriate mathematical operations. Without going into the details, these solutions can be written as

$$Q = 2(A_1/m_1 \sinh(m_1) + A_2/m_2 \sinh(m_2) + 1/M^2)$$
$$Q_p = 2(A_1 c_1/m_1 \sinh(m_1) + A_2 c_2/m_2 \sinh(m_2) + 1/M^2) \tag{3.6}$$

$$C = -m_1 A_1 \sinh(m_1) - m_2 A_2 \sinh(m_2)$$
$$C_p = -\beta\kappa(A_1 c_1 m_1 \sinh(m_1) + A_2 c_2 m_3 \sinh(m_2)). \tag{3.7}$$

Two extreme special cases can be considered. The first is when the particle phase behaves like the fluid phase at a surface, and therefore, a no slip condition for the particle phase can be

applied at the walls. The second is when the particle phase experiences perfect slip at the walls. The actual condition lies between these two extreme conditions.

For the case of no particulate slip ($\omega = 0$), the solutions for F, F_p, Q, Q_p, C, and C_p given earlier will take on the same form except the constants A_1 and A_2 will reduce to

$$A_1^* = (1 - c_2)/(M^2(c_2 - c_1)\cosh(m_1)), \qquad A_2^* = (c_1 - 1)/(M^2(c_2 - c_1)\cosh(m_2)). \tag{3.8}$$

Similarly, the same form of the solutions apply for the case of perfect particulate wall slip. However, the corresponding constants can be obtained by setting $\omega = \infty$ in equations (3.4). If this is done, A_2 and A_1 will take on the respective forms

$$A_2^{**} = (c_1 m_1 \sinh(m_1))/(M^2(c_2 m_2 \sinh(m_2)\cosh(m_1) - c_1 m_1 \sinh(m_1)\cosh(m_2)))$$
$$A_1^{**} = -(A_2^{**}\cosh(m_2) + 1/M^2)/\cosh(m_1). \tag{3.9}$$

It should be noticed that when $\omega = \infty$, the slope of the particulate axial velocity F_p at the walls will be zero. As a result, C_p will vanish as seen from equation (2.8d).

A representative set of graphical results is given in Figs 2–5 to show the influence of different physical parameters on the solutions. These are obtained by numerically evaluating equations (3.6) and (3.7). The parametric values chosen to carry out the numerical computations may or may not be intended for a specific application. In the absence of the exact form of boundary conditions to be satisfied by a particle at a surface, and due to the experimental fact that a particle experiences a certain amount of slip at a boundary, ω was set to unity so as to account for such mechanism.

Figures 2–5 display the changes in the fluid-phase volumetric flow rate Q, the particle-phase volumetric flow rate Q_p, the fluid-phase skin-friction coefficient C, and the particle-phase skin-friction coefficient C_p that are brought about by changes in both the inverse Stoke's number α and the particle loading κ, respectively. For $\kappa = 0$ (dilute suspension) the fluid-phase motion is independent of the presence of particles. Therefore, the fluid-phase physical variables in the channel such as velocity, flow rate, and the skin-friction coefficient remain unchanged even as α changes. This is clearly shown in Figs 2 and 4. As the particle loading increases, the maximum fluid and particle velocities in the channel and the slope of the fluid velocity profile at the walls decrease. As a result, Q, Q_p, and C decrease. This behavior is illustrated by the decreases in Q, Q_p, and C as κ increases shown in Figs 2–4. Figure 5 shows that the particle-phase skin friction coefficient C_p vanishes for $\kappa = 0$ and its value increases as κ increases. This is expected since C_p is defined as directly proportional to κ.

Increases in the inverse Stoke's number α have the tendency to increase the interphase

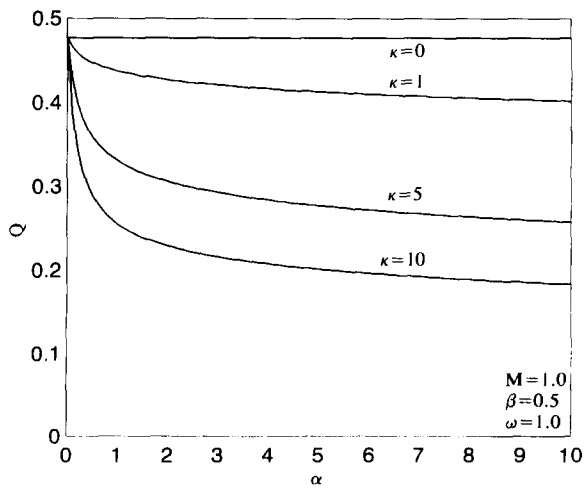

Fig. 2. Fluid-phase volume flow rate vs α.

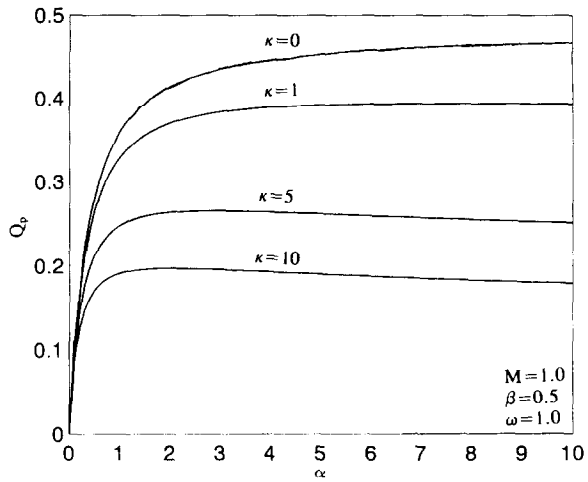

Fig. 3. Particle-phase volume flow rate vs α.

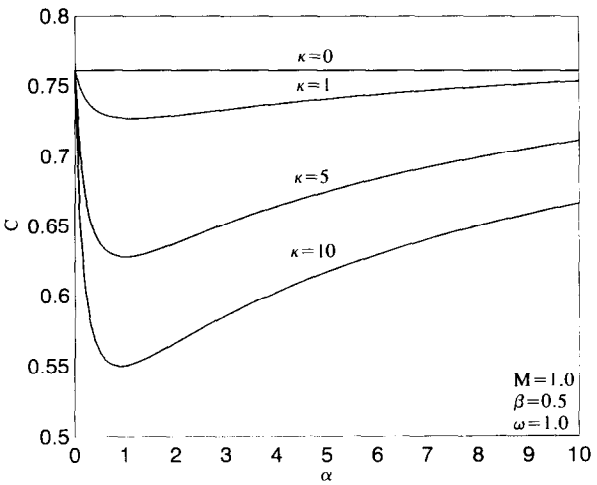

Fig. 4. Fluid-phase skin friction coefficient vs α.

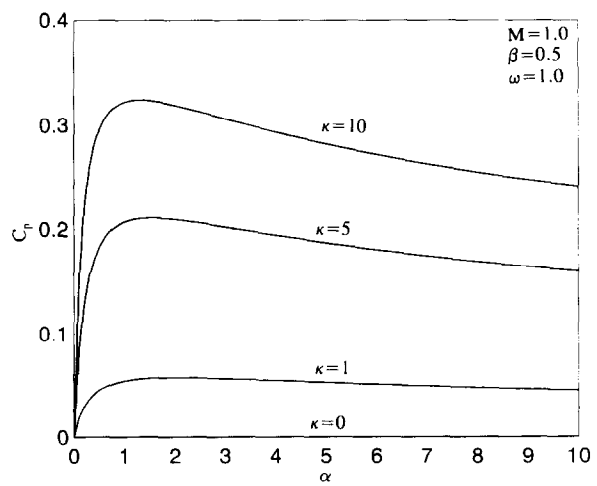

Fig. 5. Particle-phase skin friction coefficient vs α.

momentum transfer between the phases. Thus, causing the fluid-phase maximum velocity in the channel to decrease and the particle-phase maximum velocity to increase. This results in decreases in Q and increases in Q_p as α increases. For a fixed value of κ and relatively small values of α ($0 < \alpha \leq 1$), the slopes of the fluid and particle velocity profiles at the boundaries decrease and increase, respectively, yielding a corresponding reduction and increase in the values of C and C_p. However, as α is increased further, the slip velocity between the phases decreases and the slope of the fluid-phase velocity at the boundary increases as the slope of the particle-phase velocity decreases until α becomes infinite where both phases attain equilibrium conditions where both phases move together. This is represented in the respective increases and decreases in C and C_p shown in Figs 4 and 5.

3.2 Transient solutions

Equations (2.5) and (2.6) can be solved exactly subject to equations (2.7) by the separation of variables method. This is made possible by the simplifying assumptions considered in the present work. There are two approaches in which the solutions for F and F_p can be expanded. The first approach expands them in terms of series of complementary error functions (see, for instance, Schlichting [16]) while the other uses the standard trigonometric Fourier series. For convenience, the latter approach is employed by assuming that

$$F(\eta, \tau) = \sum_{n=1}^{\infty} G_n(\tau)\cos(\lambda_n \eta), \qquad F_p(\eta, \tau) = \sum_{n=1}^{\infty} G_{pn}(\tau)\cos(\lambda_n \eta) \tag{3.10}$$

where λ_n are the roots of the equation $\cos(\lambda_n \eta) = 0$ and $G_n(\tau)$ and $G_{pn}(\tau)$ are to be determined.

Differentiating equations (3.10), substituting the results into equations (2.5) and (2.6), multiplying each equation by $\cos(\lambda_m)$ (to take advantage of the orthogonality property of the cosine function), and then integrating each equation with respect to η from 0 to 1 yield

$$\dot{G}_n + (M^2 + \lambda_n^2 + \kappa\alpha)G_n - \kappa\alpha G_{Pn} = b_n \tag{3.11}$$

$$\dot{G}_{Pn} + (\beta\lambda_n^2 + \alpha)G_{Pn} - \alpha G_n = 0 \tag{3.12}$$

where a dot denotes ordinary differentiation with respect to τ and $b_n = 2(-1)^{n+1}/\lambda_n$.

Combining equations (3.11) and (3.12) into a second-order linear differential equation in G_n gives

$$\ddot{G}_n + (M^2 + \lambda_n^2(1 + \beta) + \alpha(1 + \kappa))\dot{G}_n + (\beta\lambda_n^2(M^2 + \lambda_n^2 + \kappa\alpha) + \alpha(M^2 + \lambda_n^2))G_n = (\beta\lambda_n^2 + \alpha)b_n. \tag{3.13}$$

The solution of the above linear, ordinary, non-homogeneous, differential equation subject to $G_n(0) = 0$ and $G_{Pn}(0) = 0$ can be shown to be

$$G_n = c_3 \exp(s_1 \tau) + c_4 \exp(s_2 \tau) + b_n E \tag{3.14}$$

where

$$s_1 = (-A + (A^2 - 4B)^{1/2})/2, \qquad s_2 = (-A - (A - 4B)^{1/2})/2$$

$$A = M^2 + \lambda_n^2(1 + \beta) + \alpha(1 + \kappa), \qquad B = \beta\lambda_n^2(M^2 + \lambda_n^2 + \kappa\alpha) + \alpha(M^2 + \lambda_n^2) \tag{3.15}$$

$$c_3 = -b_n(Es_2 + 1)/(s_2 - s_1), \qquad c_4 = b_n(Es_1 + 1)/(s_2 - s_1), \qquad E = (\beta\lambda_n^2 + \alpha)/B. \tag{3.16}$$

Using the solution for G_n, the corresponding solution for G_{Pn} can shown to be

$$G_{pn} = 1/(\kappa\alpha)c_3(s_1 + M^2 + \lambda_n^2 + \kappa\alpha)\exp(s_1 \tau) + c_4(s_2 + M^2 + \lambda_n^2 + \kappa\alpha) \times \exp(s_2 \tau) + b_n((M^2 + \lambda_n^2 + \kappa\alpha)E - 1). \tag{3.17}$$

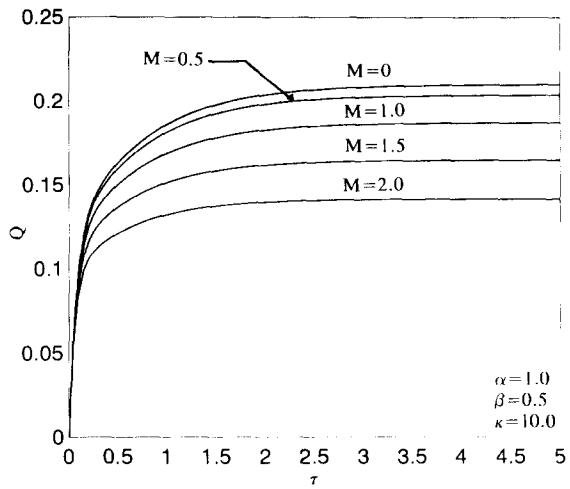

Fig. 6. Fluid-phase volume flow rate time history.

The appropriate solutions for Q, Q_p, C, and C_p are obtained by substituting equations (3.10) into equations (2.8) and performing the necessary mathematical operations to give

$$Q = 2\sum_{n=1}^{\infty}(-1)^{n+1}G_n/\lambda_n, \qquad Q_p = 2\sum_{n=1}^{\infty}(-1)^{n+1}G_{Pn}/\lambda_n$$

$$C = \sum_{n=1}^{\infty}(-1)^{n+1}\lambda_n G_n, \qquad C_p = \beta\kappa\sum_{n=1}^{\infty}(-1)^{n+1}\lambda_n G_{pn}. \tag{3.18}$$

To demonstrate the influence of the applied magnetic field on Q, Q_p, C, and C_p, equations (3.18) are numerically evaluated and the results are plotted in Figs 6–9. In these figures κ, α, and β are kept constant while M is allowed to vary.

Figures 6 and 7 illustrate the time histories of both the fluid-phase volumetric flow rate Q and the particle-phase volumetric flow rate Q_p for various values of the Hartmann number M, respectively. Increases in the values of M have the tendency to slow the motion of both the fluid and particle phases in the channel. This, in turn, causes the volumetric flow rates of both phases to decrease at any time. This is depicted in the reductions of Q and Q_p with increasing values of M shown in Figs 6 and 7. Initially at $\tau = 0$, both phases are at rest. As time progresses, and through the application of a pressure gradient, both phases begin to flow in the channel.

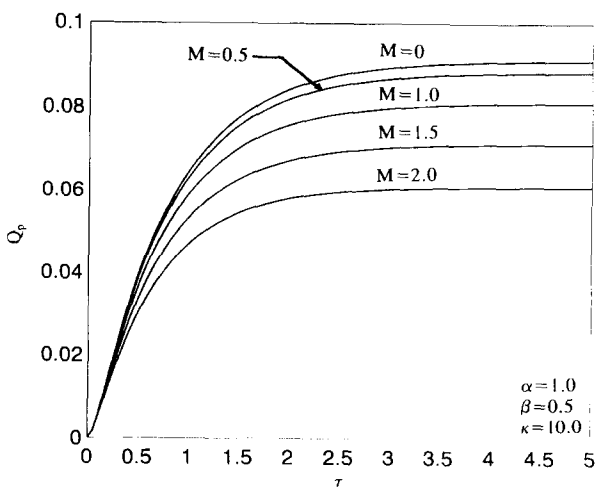

Fig. 7. Particle-phase volume flow rate time history.

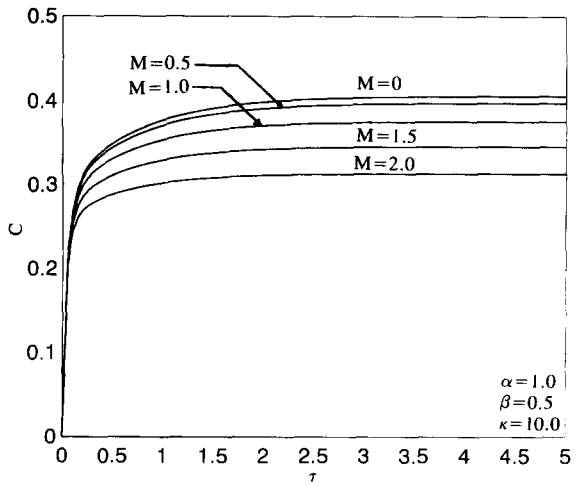

Fig. 8. Fluid-phase skin friction coefficient time history.

Thus, increasing the flow rates of both phases as evident from Figs 6 and 7. For large values of τ, the fully developed velocity profiles of both phases and consequently their flow rates will no longer change with time.

Figures 8 and 9 present the transient development of both the fluid-phase skin friction coefficient C and the particle-phase skin friction coefficient C_p for different values of M, respectively. These figures exhibit the same transient behavior as that of Q and Q_p discussed in the previous paragraph. The retardation in the motion of both the fluid and particulate phases as a result of increasing the strength of the applied magnetic field mentioned earlier causes a decrease in the slopes of both the fluid and particle velocities at the walls at any time. This is clearly illustrated by the decreases in C and C_p with increasing values of M observed in Figs 8 and 9.

It should be mentioned that all the steady-state values corresponding to the results presented in Figs 6–9 are consistent with the closed-form solutions given in equations (3.6) and (3.7) for the case of no particulate slip. Also, all unsteady results corresponding to $\beta = 0$ and $M = 0$ are in close agreement with those reported by Ritter and Peddieson [14]. Also, the steady solutions compare favorably with the results given by Tseng and Sahai [13] under the same conditions. To further check the exact solutions presented earlier for steady and time-varying conditions, the governing equations were solved numerically using a finite-difference scheme based on the

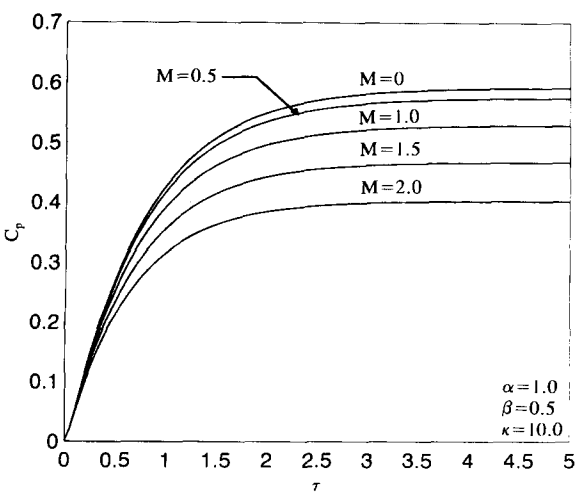

Fig. 9. Particle-particle skin friction coefficient time history.

methodology discussed by Patankar [17]. The numerical results were found to be in excellent agreement with the exact solutions. Validations of the results presented in this paper can be best accomplished by comparisons with experimental data. As far as the author is aware, such data appear to be lacking for this problem at present.

The constant volume fraction assumption employed in this problem allowed the governing equations to be solved analytically. It should be mentioned that there are more elaborate constitutive theories which predict nonuniform particulate volume fraction distributions (see, for instance, Drew and Lahey [18] and Sinclair and Jackson [19]) and, as a result, no closed-form solutions are possible.

4. CONCLUSION

Continuum equations governing two-phase particulate suspension in the presence of a transverse magnetic field are developed and applied to the problem of unsteady laminar flow in a channel. The mathematical model developed incorporates the effects of particle-phase viscous stresses, finite particulate volume fraction, and externally applied magnetic field. Steady-state and transient solutions and other limiting solutions are obtained by the usual methods of solving these kinds of equations. Numerical evaluations of the analytical solutions are performed and graphical results for the fluid-phase volumetric flow rate, the particle-phase volumetric flow rate, the fluid-phase skin-friction coefficient, and the particle-phase skin-friction coefficient are presented to illustrate the influence of the particle loading, inverse Stoke's number, and the Hartmann number on the solutions. It was found that, owing the presence of particles in the channel, the flow rates of both the fluid and particle phases are reduced. In addition, as the Hartmann number increased, the volumetric flow rates and the skin-friction coefficients of both phases decreased. While the general results obtained through the course of this work reduce to those previously published and compare well with numerically obtained results, no comparisons with experimental data were performed due to lack of existence of such data. It is hoped that the exact results presented in this paper be used as a vehicle for validation of computer routines for numerical solutions of more complicated two-phase flows.

REFERENCES

[1] F. E. MARBLE, *A. Rev. Fluid Mech.*, **2,** 397 (1970).
[2] M. ISHII, *Thermo-Fluid Dynamics Theory of Two-Phase Flow.* Eyrolles, Paris (1975).
[3] S. L. SOO, *Particulates and Continuum: Multiphase Fluid Dynamics.* Hemisphere, New York (1989).
[4] A. BERLEMONT *et al., Int. J. Multiphase Flow,* **16,** 19 (1990).
[5] A. BERLEMONT *et al., Int. J. Mass Heat Transfer,* **34,** 2805 (1991).
[6] S. L. SOO, *Appl. Scientific Res.* **21,** 68 (1969).
[7] M. GADIRAJU *et al., Mech. Res. Commun.* **19,** 7 (1991).
[8] D. A. DREW, *A. Rev. Fluid Mech.* **15,** 261 (1983).
[9] D. A. DREW and L. A. SEGAL, *Studies Appl. Math.* **50,** 233 (1971).
[10] K. R. CRAMER and S. PAI, *Magnetofluid Dynamics for Engineers and Applied Physicists.* Scripta, Washington, D.C. (1973).
[11] S. L. SOO, *Fluid Dynamics of Multiphase Systems.* Blaisdell, Waltham, Mass. (1967).
[12] J. CARSTOIU, Sylvania Elect. Prod. Eng. Note 78, Applied Research Lab. (September 1959).
[13] A. A. TSENG and V. SAHAI, *Dev. Mech.* **11,** 397 (1982).
[14] J. M. RITTER and J. PEDDIESON, *Proceedings of the Sixth Canadian Congress of Applied Mechanics* (1977).
[15] P. MITRA and P. BHATTACHARYYA, *J. Physical Soc. Jap.* **50,** 995 (1981).
[16] H. SCHLICHTING, *Boundary Layer Theory,* 4th ed. McGraw-Hill, New York (1960).
[17] S. V. PATANKAR, *Numerical Heat Transfer and Fluid Flow.* McGraw-Hill, New York (1980).
[18] D. A. DREW and R. T. LAHEY, *J. Fluid Mech.* **117,** 91 (1982).
[19] J. L. SINCLAIR and R. JACKSON, *A.I.Ch.E.J.* **35,** 1473 (1989).

(Received 3 August 1993; accepted 5 October 1993)